Published in final edited form as:
J Polym Sci B Polym Phys. 2012 May 15; 50(10): 724–737. doi:10.1002/polb.23056.

Ultra Low Density and Highly Crosslinked Biocompatible Shape Memory Polyurethane Foams

Pooja Singhal,
Biomedical Engineering Department, Texas A&M University, College Station, TX-77843, USA

Lawrence Livermore National Laboratory, Livermore CA-94550, USA

Jennifer N. Rodriguez,
Biomedical Engineering Department, Texas A&M University, College Station, TX-77843, USA

Ward Small,
Lawrence Livermore National Laboratory, Livermore, CA-94550 USA

Scott Eagleston,
Biomedical Engineering Department, Texas A&M University, College Station, TX-77843, USA

Judy Van de Water,
Division of Rheumatology, Allergy, and Clinical Immunology, University of California, Davis, CA 95616 USA

Duncan J. Maitland*, and
Biomedical Engineering Department, Texas A&M University, College Station, TX-77843, USA

Lawrence Livermore National Laboratory, Livermore, CA 94550 USA

Thomas S. Wilson*
Lawrence Livermore National Laboratory, Livermore, CA 94550 USA

Abstract

We report the development of highly chemically crosslinked, ultra low density (~0.015 g/cc) polyurethane shape memory foams synthesized from symmetrical, low molecular weight and branched hydroxyl monomers. Sharp single glass transitions (Tg) customizable in the functional range of 45–70 °C were achieved. Thermomechanical testing confirmed shape memory behavior with 97–98% shape recovery over repeated cycles, a glassy storage modulus of 200–300 kPa and recovery stresses of 5–15 kPa. Shape holding tests under constrained storage above the Tg showed stable shape memory. A high volume expansion of up to 70 times was seen on actuation of these foams from a fully compressed state. Low *in-vitro* cell activation induced by the foam compared to controls demonstrates low acute bio-reactivity. We believe these porous polymeric scaffolds constitute an important class of novel *smart* biomaterials with multiple potential applications.

Keywords

Shape Memory Polymer; Low Density Foams; Polyurethane; Aneurysm; Secondary - shape forming

Correspondence to: Duncan J. Maitland: djmaitland@tamu.edu; Thomas S. Wilson: wilson97@llnl.gov.

INTRODUCTION

Shape memory polymers (SMPs) are a fast emerging class of smart materials which can be deformed and stored in a temporary/secondary shape, and thereafter can be actuated on demand via an external stimulus, such as heat or ultraviolet light, to return to their primary shape. Several comprehensive review papers are available on the mechanism of thermally actuated shape memory behavior in polymers.[1–5] They have unique advantages over shape memory alloys such as light weight, large shape recovery of up to 400% plastic strain, non-toxicity, non-mutagenicity, ease of processing and low cost.[6] Further, a significant level of customizability of material mechanical properties is possible with polymers and multiple chemical formulations for shape memory polymers have already been reported with a wide range of mechanical properties.[1]

Processing SMPs into a porous form further increases the number of applications of these smart materials due to their unique properties including high thermal and electrical insulation, high volume changes on recovery from compressive strain (i.e. low storage volume in compressed state), and low density. SMP foams have been suggested for use in multiple commercial applications.[7] Amongst these, biomedical applications, such as tissue regeneration scaffolds and embolic foams for aneurysm occlusion, are of particular interest to us.[6, 8] Since a shape memory foam-based medical device can stay in a temporary compressed shape until it is actuated, it can be stored in a compressed state and deployed via a catheterization process. Such minimally invasive procedures can be significantly lower in cost and complications compared to the traditional open surgery. The ability to tailor their actuation temperature based on physiological requirements, and the excellent biocompatibility of polyurethane based SMPs in particular, further enhances the potential biomedical utility of SMP foams.[6]

Most of the shape memory foams reported for biomedical applications in the literature are based on a thermoplastic polyurethane developed by Mitsubishi Heavy Industries, primarily MF5520, MF6020 and MF21.[9–11] Papers on characterization of Mitsubishi polymers themselves[10–14] and some other shape memory foams[15–17] can be found. While these materials hold promise in several applications[6], some potential limitations from our perspective (i.e. for catheter-based applications) were revealed in their characterization studies. In particular, so-called “secondary-shape forming“ was noticed in which irrecoverable deformation occurred when the material was stored under compression above the glass transition temperature (Tg).[10] In other words, depending on the storage conditions (strain and temperature), the foams could partially or fully lose their capability to expand. Also, their relatively high densities provide relatively low volume expansion of 20 – 30 times.[9, 10] For a foam cylinder that does not change length, for example, this correlates to a maximum radial expansion of ~5.5 times (=√30). For aneurysm occlusion via microcatheter delivery in which the inner working diameter is ~0.5 mm, this would give a final diameter of 2.75 mm. This level of expansion may not be adequate for the proposed application: the greater the radial expansion of foam, the greater the volume that can be embolized by it for a given microcatheter inner working diameter.

Our aim in this study was to design an improved polymeric foam system directed towards biomedical applications that shows strong shape memory behavior without secondary-shape forming and volume expansion of greater than 50 times on actuation. In addition, we aimed to achieve high recovery forces, controllable actuation temperatures, good biocompatibility, and an open cell morphology for these new materials. Figure 1 gives a schematic representation of the polymer network structure of these foams. Briefly, two points form the core of this design rationale. First, secondary-shape forming in principle occurs from the relaxation of polymer chains in the secondary or deformed shape.[18, 19] So, a chemically

crosslinked structure with high density of crosslinks can potentially avoid the secondary-shape forming phenomenon by providing a permanent and strongly constrained polymer network that limits chain relaxation.[18–20] Second, for achieving a larger expansion ratio, a lower density foam is desired. Low density can potentially allow a foam sample to be compressed to smaller dimensions and thus lead to a larger volume expansion on actuation. The following materials and foaming process were considered in the development of these foams:

a. **Material choice:** Neat polymers reported by Wilson et al.[21] were used as the basis of these foams. These neat polymers made from N,N,N‘,N‘-Tetrakis(2-hydroxypropyl) ethylenediamine (HPED), 2,2',2"-Nitrilotriethanol (TEA) and 1, 6 Diisocyanatohexane (HDI), had a regular and highly chemically crosslinked network structure with low molecular weight between crosslinks.[21] These materials were developed specifically to possess high modulus ($E \sim 3n_cRT$, where E is the Young’s modulus, n_c the number crosslinks per unit volume, R the ideal gas constant and T the system temperature), high recovery stresses, sharp and controllable actuation temperatures, and strong shape memory behavior.[21] Since the density of foamed polymer has a strong effect on its modulus, $E_{porous} = E_{neat}[\rho_{porous}/\rho_{neat}]^2$ for open cell foams, where E_{porous} and E_{neat} are the Young’s moduli of porous and neat materials and ρ_{porous} and ρ_{neat} are the densities of porous and neat materials respectively,[22–24] these materials with a neat glassy modulus in the GPa range were expected to perform well at low densities. Their tight network structure with high density of covalent crosslinks was expected to limit secondary-shape forming. Also, the aliphatic monomers in this system were favorable for biocompatibility, as was demonstrated in an in-vitro study.[25]

b. **Foaming process:** A gas foaming procedure was used for the synthesis of low density foams based on highly crosslinked neat materials. Multiple techniques are available for generation of a porous polymer structure, including particulate leaching, fiber bonding, saturation with supercritical gases, high internal phase emulsion polymerization, thermally induced phase separation, stereolithography, selective laser sintering, fused deposition modeling and gas foaming.[26–33] However, most of these methods, including particulate leaching[34], stereolithography[29], selective laser sintering and fused deposition modeling, do not yield low enough densities. Thermally induced phase separation is not suitable for crosslinked systems due to the requirement of a polymer solution. High internal phase emulsion polymerization is used primarily for chain growth reactions[35] or has low control of foam structure in step growth reaction[36]. Also, use of supercritical CO_2 in foaming has poor control of foam density as the polymer crosslink density is increased.[37] Amongst these methods, gas foaming was considered to be the most promising technique for making low density foams based on polyurethane chemistry.[38–40] This technique has no direct limitations on foaming of highly crosslinked materials, and multiple additives are available commercially to modulate physical properties of the foams.

This paper presents the synthesis and characterization of these novel materials. Further, the properties of these foams are compared with other commerically available SMP foam materials to exemplify their significance and utility as a biomaterial.

EXPERIMENTAL

Foam Synthesis

N,N,N‘,N‘-Tetrakis(2-hydroxypropyl) ethylenediamine (HPED, 99%, Sigma Aldrich Inc.), 2,2',2"-Nitrilotriethanol (TEA, 98%, Alfa Aesar Inc.), 1,6-Diisocyanatohexane (HDI, TCI

America Inc.), and DI water (Millipore water purifier system, Millipore Inc., >17M ohm-cm purity), were used as received. Foams were synthesized in a three step method. First a NCO premix, or prepolymer with excess isocyanate, was made by mixing 35–40 equivalents of hydroxyl groups from varying ratios of HPED and TEA, with 100 equivalents of isocyanate groups. This NCO premix was allowed to cure for 2 days under Nitrogen. Secondly, a hydroxyl (OH) premix was made by mixing together all the balance hydroxyl groups with the surfactants and catalysts as per the amounts indicated in Table 1. Finally in the third step, the NCO premix and OH premix were mixed together in stoichiometric amounts, maintaining a 104 isocyanate index, along with the physical blowing agent, Enovate. The foam thus made was allowed to cure for at least a week before further analysis.

A series of foams with varying ratios of TEA vs. HPED in the net formulation were prepared as indicated in Table 1 to control the *Tg*. The notation H80, H60, H40, H20 and H0 denotes HPED equivalents satifying 80, 60, 40, 20 and 0 % isocyanate equivalents, respectively, excluding the 41% equivalents satisfied by water. These correspond to the neat/unfoamed compositions of A3, A5, A7, A9 and A11, respectively, as reported by Wilson et al.[21] Since the final foam density is dependent on the concentration of gas present in the foaming solution at any given time,[40] a combination of physical and chemical blowing processes was used in the foam synthesis to increase the effective concentration of gas in the foaming polymer. Also, to prevent formation of large voids in the foam in case the gas concentration goes beyond the Critical Limiting Supersaturation (CLS) level of the foaming solution,[40] simultaneous adjustment of other foaming additives, such as surfactants and catalysts, was performed to control the rate of the polymerization reaction, formation of foam cells and drainage of polymer from the cell membranes.[41] A surfactant type was chosen through qualitative consideration of monomer and blowing agent cohesive energies involving their polarity, hydrogen bonding potential and dispersive forces. For controlling the rate of isocyanate reaction with water and other hydroxyl monomers, a two catalyst system including a) a general amine-based catalyst for CO_2 generation and b) a tin-based catalyst for gelation reaction, was used. Optimization of the net formulation was done empirically with a starting point based on the supplier's (Air Products and Honeywell Corp.) foam additive specifications, and the previous literature on traditional polyurethane foams.[40] Table 1 summarizes the synthesis details of these materials for all tested compositions.

Foam Characterization

Density and Cell Structure—Core density of a representative foam sample was measured from top, middle and bottom sections of the foams as per the ASTM standard D-3574-08. Also core density of five samples from the top and middle sections was measured for each foam formulation to estimate the variation in densities across a given foam. For cell structure characterization, thin slices were cut from a representative top section of the foams, and images were captured in the brightfield mode on a Leica MZ8 microscope (Leica Microsystems Inc.) using RSImage Software (Roper Scientific Inc.).

A more in-depth cell structure analysis was done on a H60 foam sample using micro-CT imaging. The sample was imaged using a Skyscan 1172 micro-CT[42] (Micro Photonics Inc.) with a 40 kV source voltage, 250 uA source current, object to source distance of 49.48 mm and camera to source distance of 208.96 mm. These settings resulted in a reconstructed volume of foam that had a resolution of 4.15 um per voxel. For analysis of cell sizes in the reconstructed foam volume, image processing software Amira 5.3 (Visage Imaging Inc.) was used. Polar diameter (parallel to the direction of foam rise) and equatorial diameter (perpendicular to the direction of foam rise) of the ellipsoid-like cells were measured at 500 um increments throughout the volume via manual edge detection method. In all, a

cylindrical volume 6 mm in diameter and 5.12 mm high, was analyzed. Foamview software[42] was used to estimate the average strut length and pore size of the foams.

Solvent swelling and extraction—Solvent swelling and extraction experiments were carried out with Dimethylformamide (DMF; >99.8%, EMD Chemicals Inc.) as this was found to be the best solvent for such compositions.[21] Cylindrical foam samples (8 mm diameter and 2 cm height) were predried for 2 hours at 100 °C and 1 atm vacuum. The dried samples were extracted in DMF at a 25 times excess of the bulk volume of foams. Care was taken to remove the bubbles on the foam surface that can prevent adequate contact of the material with solvent. The extraction was performed on three samples of each composition for 24 hours. Post extraction the samples were vacuum dried for 24 hours at 50 °C and mass loss was measured.

Fourier transform infrared spectroscopy with attenuated total reflectance (FTIR-ATR)—The FTIR-ATR spectra was generated on a H60 foam and the corresponding neat sample using a ATR Max II reflectance accessory (Pike Technologies Inc.) on a Tensor 27 Fourier Transform Infra Red instrument (Bruker Corp.) at a 45 degree angle of incidence. 150 scans at a resolution of 4 cm^{-1} were taken in the wavenumber range of 4000 cm^{-1} to 600 cm^{-1} and background was subtracted. Testing was done in triplicate to ensure repeatability. Correction for atmospheric Water vapor and Carbon dioxide absorption was performed by subtracting respective reference spectra using the OPUS 5.5 software (Bruker Corp.).

Differential Scanning Calorimetry—*Tg* was measured using a Pyris Diamond DSC (Perkin Elmer Inc.). A 3–5 mg sample was loaded in a vented aluminum pan at room temperature, cooled to −40 °C and then run through a heat - cool - heat cycle from −40 to 120 °C. The half height of transition during second heat was taken as an estimate of the *Tg*.

Mechanical characterization

Dynamic Mechanical Thermal Analysis: For characterizing the mechanical properties of the foams as a function of temperature, a dynamic temperature ramp test was performed on a ARES-LS2 Rheometer (TA Instruments Inc.). A torsion rectangle test fixture was used on samples cut to approximately 45 mm long, 12 mm wide, and 6 mm thick with a gap distance of 25 mm. The samples were prepared by embedding both ends in a polyurethane neat polymer to prevent damage and slippage of the foam sample in the metal grips. Dynamic temperature ramp tests were then run for each formulation in triplicate, at a frequency of 1 Hz and constant heating rate of 1 °C min^{-1} from 25 to 120 °C. An initial shear strain of 0.2% was used. However, as temperature increased, it was adjusted by the control software to maintain a torque range of 0.5 to 5 g cm, allowing a maximum strain of 10% (still within the linear viscoelastic region) at high temperatures. Data points were collected every 5 seconds. Dynamic shear storage modulus (*G'*), dynamic shear loss modulus (*G"*), and their ratio tan δ (=*G"*/*G'*) were recorded using the Orchestrator™ software (TA Instruments Inc.).

Shape Memory Behavior: For measuring the shape memory behavior, constrained stress recovery tests were performed in compressive mode using parallel plate fixtures in a ARES-LS2 rheometer on H60 and H20 cylindrical foam samples (~20 mm diameter and 15 mm height). The sample was first heated up to a temperature of *Tg*+30 °C and deformed to a 80% compressive strain at a rate of 2.5 mm min^{-1}. Thereafter the sample was cooled to *Tg* −20 °C and then heated back up to *Tg*+30 °C mantaining the 80% strain. At the end of cool-heat cycle, the strain was released at a rate of 2.5 mm min^{-1} and recovered strain was measured from the distance between the plates at a 10 g axial force. Five cycles were performed on each of the three samples tested.

Effect of Storage Temperature on Shape Recovery: The behavior of stress vs. time was studied for H60 and H20 cylindrical samples (20 mm diameter and 20 mm height), using parallel plate fixtures in a ARES-LS2 rheometer. Sample size and test conditions were chosen to match the test method reported by Tobushi et al.[10] A deformation to 80% compressive strain was performed at a rate of 2.5 mm min^{-1} at Tg+30 °C temperature. The compressed sample was then brought to the test temperature, Tg+60 °C, Tg+30 °C, Tg or Tg −30 °C, and held at this temperature for 2 hours. Thereafter the temperature was brought back to Tg+30 °C and strain was released at 2.5 mm min^{-1}. The strain recovery was measured using calipers. All the compositions were tested for % shape recovery after hold at the Tg+60 °C temperature.

Maximum Volume Expansion: Maximum volume expansion for foam samples was measured using a SC150-42 Stent Crimper (Machine Solutions Inc.). Cylindrical foam samples 6 mm in diameter were loaded in the crimper and compressed as small as possible, at Tg+30 °C, by setting the target diameter to zero. They were then allowed to cool down to room temperature to fix the compressed shape. The actual compressed diameter was measured using a digital micrometer. Finally, the samples were heated back to Tg+30 °C in air, and the recovered diameter was measured using calipers. Net volume expansion was calculated (ignoring any change in length) as follows:

$$Volume\ expansion = (recovered\ diameter / compressed\ diameter)^2$$

Biocompatibility Study—*In vitro* biocompatibility testing was performed to estimate the biological response of these foams. Representative H80 foam samples were first cut into discs of approximately 12 mm diameter and 2 mm thickness, and then cleaned and sterilized using ethylene dioxide gas. Biocompatiblity was evaluated by measuring cytokine expression as per Cabanlit et al.[25] Blood of 5 female and 5 male human subjects was used following the approved human subject protocol 993120, University of California, Davis. Peripheral blood from these subjects was collected and stored in citrate tubes which allowed the stabilization of pertinent cell populations of the cell culture. Next, the collected blood samples were centrifuged at 3000 rpm for 10 minutes and the supernantant plasma was separated. For testing the material biocompatibility, SMP foam discs were incubated using X-vivo media (serum-free medium; Cambrex Corp.) and 1:1 plasma-free whole blood. Positive controls included two mitogens, lipopolysaccharide (LPS, Sigma-Aldrich) and phytohemagglutinin (PHA, Sigma-Aldrich Inc.), added to the whole blood cultures at amounts of 25 μg mL^{-1} and 50 μg mL^{-1} respectively. As a measure of the background activation, a control test of cells incubated in media without SMP foam material was performed. The samples were kept incubated at 37 °C in 24-well plates for a duration of 48 hours. This duration was chosen to allow measurable production of all cytokines, including those derived from T lymphocytes.

After the 48 hour incubation, the culture supernatants were collected and stored at −20 °C. These were then tested with an enzyme-linked immunosorbent assay (ELISA, Duoset ELISA Development System kits (R&D Systems Inc.)) for TNF-α, IL-1β, IL-6, IL-8, and IL-12 according to the manufacturer's instructions. Optical density readings at 570 nm were subtracted from those at 450 nm to account for optical imperfections. Mean optical density was recorded for TNF-α, IL-1β, IL-6, IL-8, and IL-12 over duplicate sample runs. A standard linear curve of optical density reading versus concentrations (pg mL^{-1}) on a log −log scale was used to convert optical density values to concentrations, and their average and standard deviations were calculated. P-values (one-tailed t-test) were calculated to determine if cell activation was significantly higher compared to the media alone (0.05 significance level).

RESULTS AND DISCUSSION

Density and cell structure

Table 1 shows the composition of different foams analyzed in this study, and representative densities of the foams are reported in Table 2. Average densities of 0.021±0.002, 0.019±0.001, 0.016±0.001, 0.021±0.001 and 0.020±0.005 g cm^{-3} were recorded for foam compositions of H0 through H80 respectively over five samples in the top and middle sections. These correspond to an average porosity [= ($\rho_{neat} - \rho_{porous}$)/$\rho_{neat}$] of ~98 % and a high average theoretical volume expansibility (= $\rho_{neat}/\rho_{porous}$) of 64 ± 9 times; here ρ_{neat} ~1.174 g cm^{-3} is the neat polymer density, and ρ_{porous} is the foam density. The small variation in densities in middle and top sections of the foam indicates a fairly uniform structure. Comparatively higher density is seen in the bottom section of foams in some cases. This is attributed to the effect of gravity on the rising foams as is typically seen in blown foams[43], and is accounted for in the foam characterization by taking the top/middle areas of the foams for the characterization tests.

Optical microscopy (Figure 2) shows a mixed closed to open cell structure for these foams, with thin residual membranes on the foam cells. Here the terms open or closed cell should be considered with reservations. Since some texts classify foams into just two categories of closed and open cells[40], and others classify them into three categories of closed, open and reticulated cells[44], these terms can be ambiguous. Generally, blown foams have been found to retain thin residual membranes post-synthesis, and removal of these membranes (up to 97%) to make foams completely open cell or reticulated invariably requires secondary physical processes such as hydrolysis, oxidation, heat or mechanical treatment.[40] Here, we classify these as-processed foams as effectively closed cell, or mixed closed to open cell, due to the presence of cell membranes which may impede the free movement of blood or interstitial fluid through the foam.

Some variation in the average cell size was seen for foams across different formulations (Figure 2). This could be due to the different hydrophobicity, or different viscosity of the foaming solutions across the formulations at varying ratios of HPED and TEA. Indeed, in an ongoing separate study in which the viscosity of the foaming solution was the manipulated parameter, cell sizes of resulting foams could be precisely controlled, and were generally seen to decrease with increase in the viscosity of the foaming solution. Figure 3 shows a histogram of cell size distribution within a H60 foam sample. Its pore cells were found to be anisotropic as is typically seen for blown foams.[40] They were approximately 1000 μm tall in the direction of free-rise during foaming, and 700 μm wide. Using the image analysis software Foamview[42], the H60 foams were found to have strut length of approximately 400 μm, and an average pore volume of 7×10^8 μm^3.

Currently in the literature low density foams have been reported mostly down to the lower limit of 0.02–0.03 g cm^{-3}. Some foams with densities down to 0.006 g cm^{-3} have been reported, but a high amount of water (~75 wt %) was used in their synthesis.[45] This is not preferable for our application, as using high amounts of water as a chemical blowing agent will interfere with the desired chemically crosslinked network structure of the material. Also foams with densities down to 0.016 g cm^{-3} have been achieved by varying the polyol type and amounts.[46] However, to our knowledge, SMP foams with densities less than 0.02 g cm^{-3} have not been previously reported. Also, low density SMP foams with a network structure involving such high density of chemical crosslinks have not been reported.

Solvent swelling and extraction

Solvent extraction results for all foam formulations are given in Table 2. The foam samples were all well swollen and without air bubbles in the DMF media. Results show that

approximately 96 to 99% of the initial monomers were incorporated into the polymer network. The composition of the soluble fraction was not determined, but it is expected to be a combination of residual foaming additives, such as surfactants and catalysts, and impurities in the original monomers. Also, some mass loss was apparent from slight mechanical damage to the foams incurred during removal of bubbles. This indicates that >85% of functional groups were consumed in reaction[21] and that the resulting network is indeed a highly crosslinked one.

Fourier transform infrared spectroscopy with attenuated total reflectance (FTIR-ATR)

FTIR-ATR of a H60 foam and corresponding neat polymer is shown in Figure 4a. The neat polymer spectra is offset by 0.03 absorbance units with respect to the foam spectra for clarity. Details of the peak assignment in polyurethane foams can be found in other references.[47–50] The absorption spectra showed a strong C=O urethane peak at 1689 cm^{-1}. A C=O peak has previously been reported for polyurethanes at 1703–1710 cm^{-1} [49], 1694 cm^{-1} [50] and 1706–1713 cm^{-1} [47] for hydrogen bonded urethane, and 1730–1740 cm^{-1} [49], 1729–1739 cm^{-1} [47] and 1725 cm^{-1} [50] for free urethane. Hence a shift of C=O peak to 1689 cm^{-1} in these foams suggests a more strongly hydrogen bonded structure than is seen with previously reported polyurethane foams.[47–50] Based on the molecular structure of these foams, an average theoretical molecular weight between chemical crosslinks can be calculated as 270–440 g mol^{-1}. Further, approximately 2–3 urethane and/or urea bonds may be present between the chemical crosslinks for every segment. Hence these foams are expected to develop a high density of hydrogen bonds, which explains the shift of the urethane peak to a lower wavenumber in the FTIR spectra. This is in contrast with the traditional polyurethane foams, which typically have base polyols with molecular weights in the range of a few thousand grams per mole[40]. Two important differences are seen between the spectra of the neat polymer and foam: 1) presence of a shoulder in the 1620–1660 cm^{-1} range indicating presence of urea linkages in the foam from the use of water as a chemical blowing agent (Figure 4b) and 2) a comparatively broader peak from 3100–3500 cm^{-1} in the foam indicating increased hydrogen bonded N-H vibrations (Figure 4c).[50] Polyurea segments are reported to show characteristic absorption at 1690–1700 cm^{-1} in free form, 1660–1670 cm^{-1} in disordered hydrogen bonded form, and 1630–1645 cm^{-1} in ordered hydrogen bonded form.[47] The urea shoulder suggests a peak at ~1650 cm^{-1} (Figure 4b) indicating presence of hydrogen bonding in the urea segments but not quite as strong as that found in ordered urea segments. This may be due to the high crosslink density that can interfere with the alignment of urea bonds, and prevent formation of as strong a hydrogen bonding as is typically found in the hard segments of polyurethanes.

Differential scanning calorimetry (DSC)

DSC curves of these foams are shown in Figure 5. Results show that glass transition/ actuation temperature (*Tg*) could be precisely controlled in the functional range of 44–69 °C by varying the ratio of HPED to TEA in the foam formulation (Figure 5, Table 2). A higher content of HPED gave a higher *Tg*. This agrees well with the results of Wilson et al.,[21] and can be due to the secondary hydroxyl group of HPED, which positions a methyl group adjacent to the urethane bond. This methyl group can present steric hinderance to rotational motion around the urethane linkage and increase the *Tg*. Also HPED has a functionality of four which gives a higher crosslink density to the polymer structure, and can increase its *Tg* in comparison to trifuncional TEA. However, the transition values don't exactly match the respective compositions in Wilson et al.[21] This can be explained from the use of water as a chemical blowing agent, which introduces urea groups in the network and thereby increases the *Tg*. Also, the *as synthesized* foam samples can have some residual foaming additives, such as surfactants and catalysts, that can possibly lead to a decrease in *Tg* by plasticization.

We are currently working on understanding the effect of urea bonds and residual foaming additives in more detail for blown foams.

Mechanical properties

Dynamic Mechanical Thermal Analysis—The dynamic temperature ramp test results are shown in Figure 6. A drop in modulus is observed across the Tg of the foam, going from 200–300 kPa in the glassy state to 5–15 kPa in the rubbery state. Values of G' in the rubbery and glassy states, T_{onset} (temperature at the intersection of the baseline and leading edge of the peak in $tan\,\delta$), $T_{\delta s}$ (temperature at the peak in $tan\,\delta$), ΔT (breadth of transition = $2(T_{\delta s} - T_{onset})$ according to Yackaki et al.[51]) and $tan\,\delta$ values at $T_{\delta s}$ for all formulations are given in Table 2. The rubbery state modulus of shape memory polymers is a measure of force of recovery on actuation, and the ratio of the glassy state to the rubbery state modulus, defined as $G'(Tg - 20\ °C)/G'(Tg + 20\ °C)$, is an indicator of the shape fixity of an SMP.[21] The modulus of these foams drops by ~30 times across the transition. While this is not as high as reported for other SMPs in general, shape memory behavior is still quite strong for these foams (Figure 7), particularly for such low densities. A trade-off that comes with the high modulus values and highly crosslinked network structure of these foams is the limited elongation at failure (~35% for neat unfoamed films).[21] But with the typically polyhedral shape of the foam cells, individual cell struts undergo only small tensile strains during compression, as they are made to bend and align together. Hence the low net elongation to failure is acceptable for the proposed applications of these foams.

It is noteworthy that the shear storage modulus is found to approximately scale with the density in accordance with $G'_{porous} = G'_{neat}(\rho_{porous}/\rho_{neat})^2$ in the glassy regime, which has been shown to be true for ideal open cell foams.[24, 52] Here ρ_{neat} ~1.174 g cm^{-3}, G'_{neat}= 700–905 MPa, and average ρ_{porous}~ 0.019 g cm^{-3}, yielding calculated G'_{porous}=183–237 kPa. This result is in good agreement with the measured average G'_{porous} ~212–260 kPa,1 indicating that these foams have primarily an open cell behavior from a mechanical standpoint. This is consistent with the cell structure images, and confirms that although cell membranes are present they are sufficiently thin and do not affect the mechanical behavior of the foam significantly.

Shape Memory Behavior—Five shape memory cycles on a H20 foam sample are shown in Figure 7. A typical shape memory response is seen in a cycle of four key steps, as depicted in Figure 7a. The first step of ***Loading*** shows an increase in stress as the sample is deformed to 80% compressive strain at Tg+30 °C. The second step of ***Fixing*** reduces the stress rapidly across the Tg as the sample is cooled from Tg+30 °C to Tg–20 °C. The third step of constrained ***Stress recovery*** increases the stress back up to ~10 kPa via heating to Tg +30 °C. Finally the fourth step of ***unloading*** reduces the stress to zero as the strain is removed, and the foam recovers its primary shape.

Figure 7b and 7c show the behavior of stress vs. strain and stress vs. temperature for 5 shape memory cycles on these foams, respectively. The first cycle shows the highest stress values, followed by the second cycle, and thereafter all the cycles show significant overlap. Hysteresis in the initial cycles is presumed to be from the changes in the macrostructure of foams, such as breaking of some cell membranes or damage to cell struts. Also changes at the microstructural level due to residual stresses in the material and re-arrangement of side groups and dangling ends in the polymer can contribute to hysteresis.[21] An average recovery

[1]Here the neat polymer density and modulus are taken from the corresponding formulations in Wilson et al.[21] It is to be noted that the neat polymer density and modulus do not account for the effect of water in the foam composition which affects the chemical crosslink density of the material. However, the actual neat density and modulus may not be very different for the foam material due to strong hydrogen bonding of urea groups which compensates for the loss of chemical crosslinks.

of 92±2%, 95±3%, 96±1%, 97±1% and 97±1% was measured in cycles 1 through 5 respectively, over 3 samples for H20 samples. For H60 samples these values were 93±2%, 95±1%, 97±1%, 97±1%, 97±1% respectively. High strain recovery in later cycles demonstrates close to an ideal spring behavior, consistent with the low values of $tan\,\delta$ of these foams (Table 2).

The stress values of ~ 10–22 kPa as seen in Figure 7 may seem low compared to the typical values of polymeric foams. However, their low density of 0.018 g cm^{-3} as well as rubbery state should be considered. By calculating the corresponding stresses for these foams at higher densities using known scaling relationships, we can compare them to other published SMP foams under similar test conditions. Ashby and Gibson[24, 52] demonstrated that the compressive stresses of a wide range of flexible and rigid polymer foams scale approximately with the material density as follows (valid for open cell foams with $\frac{\rho_{porous}}{\rho_{neat}}<0.3$)[24, 52]: $\sigma_{el} \propto \left(\frac{\rho_{porous}}{\rho_{neat}}\right)^2; \sigma_{pl} \propto \left(\frac{\rho_{porous}}{\rho_{neat}}\right)^{\frac{3}{2}}$ where σ_{el} and σ_{pl} are the stresses in elastic and plastic deformation regimes, and ρ_{porous} and ρ_{neat} are densities of porous and neat forms of polymer, respectively. Since the strain of shape memory materials is largely recoverable, the compressive stresses should be valid in the non-linear elastic deformation regime (i.e. σ_{el}), but both σ_{el} and σ_{pl} are considered here for a more complete comparison.

A commercial thermoset epoxy foam (density 0.2 g cm^{-3}), for instance, was reported to have stress of ~38 kPa at 60% compressive strain at 30 °C above *Tg*.[16] Compressive stress of the foam reported here is ~4.5 kPa under similar conditions (Figure 7b). As a comparison, values of σ_{el} and σ_{pl} for these foams at 0.2 g cm^{-3} density would scale to ~556 kPa and 167 kPa based on the above relations. Polyether polyol based polyurethanes reported by Domeier et al. (density 0.21 g cm^{-3}) showed peak recovery stresses in the range of 1000 kPa on 80% compressive strain at *Tg*.[15] Stresses for the foams reported here are ~15 kPa under similar conditions except that compression for these was done at *Tg*+30 °C. This would scale to σ_{el}~2000 kPa and σ_{pl}~598 kPa for a density of 0.21 g cm^{-3}. A polyether polyol series polyurethane foam from Mitsubishi Industries, MF6020, (density of approximately 0.032 g cm^{-3} [6]) reported about 48 kPa compressive stress at 80% strain at 30 °C above *Tg*.[10] The foams reported here have stresses of ~15 kPa under similar conditions, and would scale to σ_{el}~47 kPa and σ_{pl}~36 kPa, respectively. Hence after accounting for the low densities, recovery stresses of these materials are seen to be significantly higher or comparable to other reported SMP foams. It is noteworthy that the number of cycles, strain rate, compressive strain and temperature can all have an effect on the compressive stresses measured for a foam sample. Hence while these results give an estimate of the expected stress range, their exact values could change with changes in the processing conditions.

Effect of Storage Temperature on Shape Recovery—The stress response of H20 foam samples as they were held under compression over a 2 hour period at different temperatures, is shown in Figure 8. In the first step of ***loading*** to 80% compressive strain at *Tg*+30 °C, all four samples showed a similar increase in stress, as expected (Figure 8a). In the second step of ***hold***, the samples were taken to their respective test temperatures of *Tg* −30 °C, *Tg*, *Tg*+30 °C and *Tg*+60 °C, and an initial stress relaxation was seen (Figure 8b). The extent of this relaxation was higher for samples held above *Tg* compared to the sample held at *Tg*. This is expected from the higher mobility of polymer chains at higher temperatures. The sample held at *Tg*−30 °C also showed a large drop in stress, which can be explained with the thermal contraction and storage of internal energy and entropy[20] in the glassy state of the polymer, akin to the ***fixing*** step of a shape memory cycle. Beyond the initial relaxation, the stresses were held largely constant throughout the hold of 2 hours at the test temperature (Figure 8b). Finally in the third step of ***unloading***, a decrease in stress

was recorded as the strain was released at *Tg*+30 °C (Figure 8c). An initial increase in stress was noticed for the sample stored at *Tg*−30 °C during strain recovery, possibly due to a lag in the heating of the sample even as the crosshead moved to release the strain. A net shape recovery of 94, 93, 96, and 98% was measured for H20 (Tg~50 °C) samples held at temperatures of *Tg*+60 °C, *Tg*+30 °C, *Tg*, and *Tg*−30 °C, respectively. For H60 (Tg~60 °C) samples these values were 95, 91, 98 and 96% respectively. % shape recovery after holding under 80% compressive strain for 2 hours at Tg+60 °C, for all the compositions, is reported in Table 2.

In contrast to the results above, physically crosslinked materials, such as polyether polyol based MF6020 (Tg~60 °C) foams[10], have been reported to show ~8–10% residual strain for hold at Tg+30 °C, and ~100% residual strain (0% shape recovery) for hold at *Tg*+60 °C for 2 hours at 80% compressive strain.[10] Generally, as the applied strain and storage temperature decreased, the extent of secondary-shape forming was seen to decrease for these physically crosslinked foams. Also, Di Prima et al. reported ~ 40% strain recovery after compression to 80% strain at 125 °C (~*Tg*+33 °C) in proprietary epoxy based foams.[16] The foams based on a chemically crosslinked network reported here show significantly higher shape recovery in comparison.

Assuming that the above materials are thermally stable at the tested temperatures, this can be explained from the effect of covalent crosslinks on polymer chain relaxation.[18, 20] The covalent crosslinks in this system can be considered permanent over the conditions and time scales investigated. While network chain segments can conformationally rearrange above *Tg*, their ends remain attached to the same network junction point. This constrains the equilibrium arrangement of crosslink points and thus the equilibrium shape of the material. In contrast, the physical crosslinks, such as in segmented polyurethanes, are labile. Here entropically driven polymer chains can move in and out of the physical crosslinks to achieve a more favorable, lower energy state.[19, 53] Since the rate of this conformational rearrangement of chains is dependent on their mobility, it would occur over increasingly long time scales as temperature is decreased below *Tg*, and at shorter time scales at temperatures above *Tg* where the mobility of the chains is high. As the polymer chains relax/re-arrange to an equilibrium conformation while the material is held in the secondary shape, the *memory* of the primary shape is erased, and a residual strain or phenomenon of secondary-shape forming is observed. Hence, the high shape recovery of the reported materials, after storage at *Tg*+60 °C for 2 hours, is consistent with their network structure comprising high density of covalent crosslinks.

However, if a chemical reaction occurs in the material at high temperatures, new bonds can form resulting in loss of shape memory of the polymer for both physically and chemically crosslinked materials. While SMPs are not meant to be stored at temperatures above their *Tg*, the improved shape holding of these materials at temperatures above Tg, compared to the other physically crosslinked foams, suggests an advantage of improved shelf life during storage in their secondary shape below Tg.

Maximum Volume Expansion—Volume expansion measured for the foam samples are reported in Table 2. 6 mm diameter cylindrical foam samples were radially compressed (2-D deformation) to an average minimum diameter of 0.68 mm. On recovery, close to the theoretical volume expansion of up to an average of 68 times was seen. This is an improvement of more than a factor of two compared to other reported shape memory polymer foams.[9, 10] Figure 9 demonstrates the change in the physical form of a foam sample as it expands in a fluid media from a fully compressed shape.

Biocompatibility Study

Results of the in-vitro biocompatibility study of these foams is reported in Table 3. Biocompatibility was analyzed based on the level of cytokine production from the cells cultured on the foam and control substrates. The positive controls (PHA- and LPS-stimulated cells) demonstrated significantly higher cell activation compared to the media alone ($p<0.05$). Activation of IL-1β, IL-6, IL-8, and TNF-α for the foam was not significantly higher than that for the media alone ($p>0.05$ in all cases), though average values appear somewhat elevated for IL-1β, IL-6, and IL-8. Activation of IL-12, although significantly different compared to the media alone ($p<0.05$), was only marginally higher. Overall, the relatively low cell activation induced by the foam suggests promising biocompatibility. These in vitro results are supported by a recent publication that includes pilot 90-day implant results of a related foam formulation, in a vein pouch carotid aneurysm model (porcine).[54] The in vivo study showed low inflammation and good healing in two foam-treated aneurysms in a single animal.

CONCLUSIONS

1. Novel polyurethane shape memory polymer foams were synthesized based on small molecular weight branched monomers to get a highly chemically crosslinked network structure with low molecular weight between crosslinks. Swelling and extraction studies showed a highly crosslinked structure with 96–99% of mass incorporated in the network. Furthermore, extensive hydrogen bonding was deduced from the FTIR results. The actuation temperature of the foams could be customized in the range of 45–70 °C by changing the composition of constituent monomers.
2. Very low densities (~0.015–0.021 g cm^{-3}) were achieved in these foams. They had a mixed, closed to open cell morphology, with thin residual cell membranes.
3. The materials showed high glassy storage modulus of 200–300 kPa even at such low densities. Excellent shape recovery of 97–98% was recorded for these materials post initial conditioning cycles, and up to a 70 times volume expansion was seen which is a significant improvement over other known SMP foams.
4. The drawback of secondary-shape forming above Tg seen in the traditional physically crosslinked foams was significantly reduced through a high density of covalent crosslinks in the structure. Shape recovery of 94% (for Tg~50 °C) and ~95% (for Tg~60 °C) was achieved for these foams in contrast to ~0% shape recovery of physically crosslinked foams (Tg~60 °C) under similar storage conditions (80% compressive strain at Tg+60 °C for 2 hours). Although conditions of higher temperatures, longer holding times and larger strains are not investigated in detail here, this result suggests an improved shelf life of these foams for storage in a compressed secondary shape below Tg.

The polyurethane foams reported here are, to our knowledge, unprecedented in the aspect that they simultaneously show a very highly crosslinked polymeric structure and very low material densities down to 0.015 g cm^{-3}. These unique properties, in addition to the encouraging *in vitro* biocompatibility results, suggest that these foams are particularly promising as biomaterials for embolic devices in minimally invasive medical applications.

Acknowledgments

This work was partially performed under the auspices of the U.S. Department of Energy by Lawrence Livermore National Laboratory under Contract DE-AC52-07NA27344 and supported by the National Institutes of Health/ National Institute of Biomedical Imaging and Bioengineering Grant R01EB000462 and by Lawrence Livermore

National Laboratory Directed Research and Development (LDRD) Grants 04-LW-054 and 04-ERD-093. The authors would like to thank Benjamin Ache and Arun Tatiparthi from Micro Photonics Inc. for micro-CT imaging and technical assistance.

REFERENCES AND NOTES

1. Liu C, Qin H, Mather P. J. Mater. Chem. 2007; 17(16):1543–1558.
2. Lendlein A, Kelch S. Angew. Chem. Int. Ed. 2002; 41(12):2034–2057.
3. Mather PT, Luo X, Rousseau IA. Annu. Rev. Mater. Res. 2009; 39:445–471.
4. Rousseau IA. Polym. Eng. Sci. 2008; 48(11):2075–2089.
5. Behl M, Lendlein A. Mater. Today. 2007; 10(4):20–28.
6. Metcalfe A, Desfaits AC, Salazkin I, Yahia LH, Sokolowski WM, Raymond J. Biomaterials. 2003; 24(3):491–497. [PubMed: 12423604]
7. Sokolowski, WM.; Hayashi, S. presented at the Proceedings of the SPIE. Smart Structures and Materials: Smart Structures and Integrated Systems in San Diego (USA); 2003. p. 534-544.
8. Small W IV, Singhal P, Wilson TS, Maitland DJ. J. Mater. Chem. 2010; 20(17):3356–3366. [PubMed: 21258605]
9. Hayashi, S.; Fujimura, H. Patent No. 5,049,591. 1991.
10. Tobushi H, Matsui R, Hayashi S, Shimada D. Smart Mater. Struct. 2004; 13:881–887.
11. Tobushi H, Okumura K, Endo M, Hayashi S. J. Intell. Mater. Syst. Struct. 2001; 12(4):283–287.
12. Tobushi H, Hashimoto T, Ito N, Hayashi S, Yamada E. J. Intell. Mater. Syst. Struct. 1998; 9(2): 127–136.
13. Tobushi H, Hayashi S, Kojima S. JSME Int. J I-Solid. M. 1992; 35(3):296–302.
14. Tobushi H, Hara H, Yamada E, Hayashi S. Smart Mater. Struct. 1996; 5:483–491.
15. Domeier L, Nissen A, Goods S, Whinnery LR, McElhanon J. J. Appl. Polym. Sci. 2010; 115(6): 3217–3229.
16. Prima M, Di, Lesniewski M, Gall K, McDowell D, Sanderson T, Campbell D. Smart Mater. Struct. 2007; 16:2330–2340.
17. Nardo LD, Bertoldi S, Tanzi MC, Haugen HJ, Farè S. Smart Mater. Struct. 2011; 20(3) 035004.
18. Cernošek Z, Holubová J, Cernošková E, Liška M. J. Optoelectron. and Adv. Mater. 2002; 4(3): 489–503.
19. Nguyen TD, Jerry Qi H, Castro F, Long KN. J. Mech. Phys. Solids. 2008; 56(9):2792–2814.
20. Gall K, Yakacki CM, Liu Y, Shandas R, Willett N, Anseth KS. J. Biomed. Mater. Res. A. 2005; 73(3):339–348. [PubMed: 15806564]
21. Wilson T, Bearinger J, Herberg J, Marion J III, Wright W, Evans C, Maitland D. J. Appl. Polym. Sci. 2007; 106(1):540–551.
22. Egli E. J. Cell. Plast. 1972; 8(5):245–249.
23. Progelhof R, Throne J. Polym. Eng. Sci. 1979; 19(7):493–499.
24. Gibson L, Ashby M. P. Roy. Soc. Lond. A Mat. 1982; 382(1782):43–59.
25. Cabanlit M, Maitland D, Wilson T, Simon S, Wun T, Gershwin ME, Van de Water J. Macromol. Biosci. 2007; 7(1):48–55. [PubMed: 17238230]
26. Freyman T, Yannas I, Gibson L. Prog. Mater Sci. 2001; 46(3–4):273–282.
27. Hacker M, Ringhofer M, Appel B, Neubauer M, Vogel T, Young S, Mikos AG, Blunk T, Göpferich A, Schulz MB. Biomaterials. 2007; 28(24):3497–3507. [PubMed: 17482257]
28. Mikos AG, Temenoff JS. Electron. J. Biotechno. 2000; 3(2):23–24.
29. Cooke MN, Fisher JP, Dean D, Rimnac C, Mikos AG. J. Biomed. Mater. Res., Part A. 2003; 64(2): 65–69.
30. Pham QP, Sharma U, Mikos AG. Tissue Eng. 2006; 12(5):1197–1211. [PubMed: 16771634]
31. Cooper AI. Adv. Mater. 2001; 13(14):1111–1114.
32. Busby W, Cameron NR, Jahoda CAB. Biomacromolecules. 2001; 2(1):154–164. [PubMed: 11749167]

33. Harris LD, Kim BS, Mooney DJ. J. Biomed. Mater. Res. 1998; 42(3):396–402. [PubMed: 9788501]
34. Shi X, Sitharaman B, Pham QP, Liang F, Wu K, Edward Billups W, Wilson LJ, Mikos AG. Biomaterials. 2007; 28(28):4078–4090. [PubMed: 17576009]
35. Christenson EM, Soofi W, Holm JL, Cameron NR, Mikos AG. Biomacromolecules. 2007; 8(12): 3806–3814. [PubMed: 17979240]
36. David D, Silverstein MS. J. Polym. Sci., Part A: Polym. Chem. 2009; 47(21):5806–5814.
37. Jacobs L, Kemmere M, Keurentjes J, Mantelis CA, Meyer T. AIChE Journal. 2007; 53(10):2651–2658.
38. Elwell MJ, Mortimer S, Ryan AJ. Macromolecules. 1994; 27(19):5428–5439.
39. Elwell MJ, Ryan AJ, Gruenbauer HJM, Van Lieshout HC. Macromolecules. 1996; 29(8):2960–2968.
40. Klempner, D.; Sendijarevic, V.; Aseeva, RM. Handbook of polymeric foams and foam technology. Hanser Gardner Publications; 2004.
41. Shah D, Djabbarah N, Wasan D. Colloid. Polym. Sci. 1978; 256(10):1002–1008.
42. Montminy MD, Tannenbaum AR, Macosko CW. J. Colloid Interf. Sci. 2004; 280(1):202–211.
43. Jackovich D, O'toole B, Hawkins MC, Sapochak L. J. Cell. Plast. 2005; 41(2):153–168.
44. Webster, JG. Prevention of pressure sores - Engineering and clinical aspects. New York: Taylor and Francis group; 1991.
45. Burdeniuc, JJ.; Andrew, GD. Patent No. US. 2010/0152312 A1. 2008.
46. Haider, K.; Steppan, D.; Mcgregor, M.; Ingold, K.; Mautino, V.; Drobransky, M. WO Patent. WO/2004/000,907. 2003.
47. Ning L, De-Ning W, Sheng-Kang Y. Macromolecules. 1997; 30(15):4405–4409.
48. Yang B, Huang WM, Li C, Li L. Polymer. 2006; 47(4):1348–1356.
49. YIlgör E. Polymer. 2002; 43(24):6551–6559.
50. Zhang L, Jeon HK, Malsam J, Herrington R, Macosko CW. Polymer. 2007; 48(22):6656–6667.
51. Yakacki CM, Shandas R, Safranski D, Ortega AM, Sassaman K, Gall K. Adv. Func. Mater. 2008; 18(16):2428–2435.
52. Ashby M, Medalist R. Metall. Mater. Trans. A. 1983; 14(9):1755–1769.
53. Mcgonigle EA, Cowie J, Arrighi V, Pethrick R. J. Mater. Sci. 2005; 40(8):1869–1881.
54. Rodriguez J, Yu Y-J, Miller M, Wilson T, Hartman J, Clubb F, Gentry B, Maitland D. Ann. Biomed. Eng. 2011

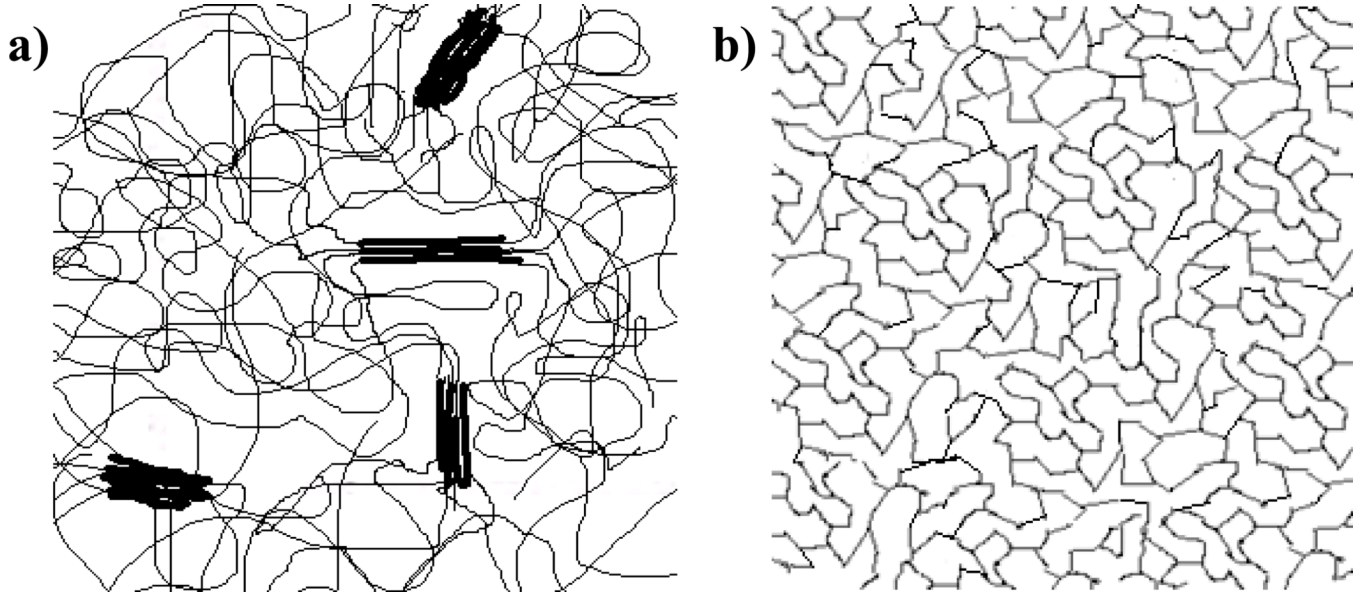

Figure 1.
A schematic representation of the network structure of (a) physically crosslinked traditional polyurethane foams and (b) proposed chemically crosslinked foams from low molecular weight monomers.

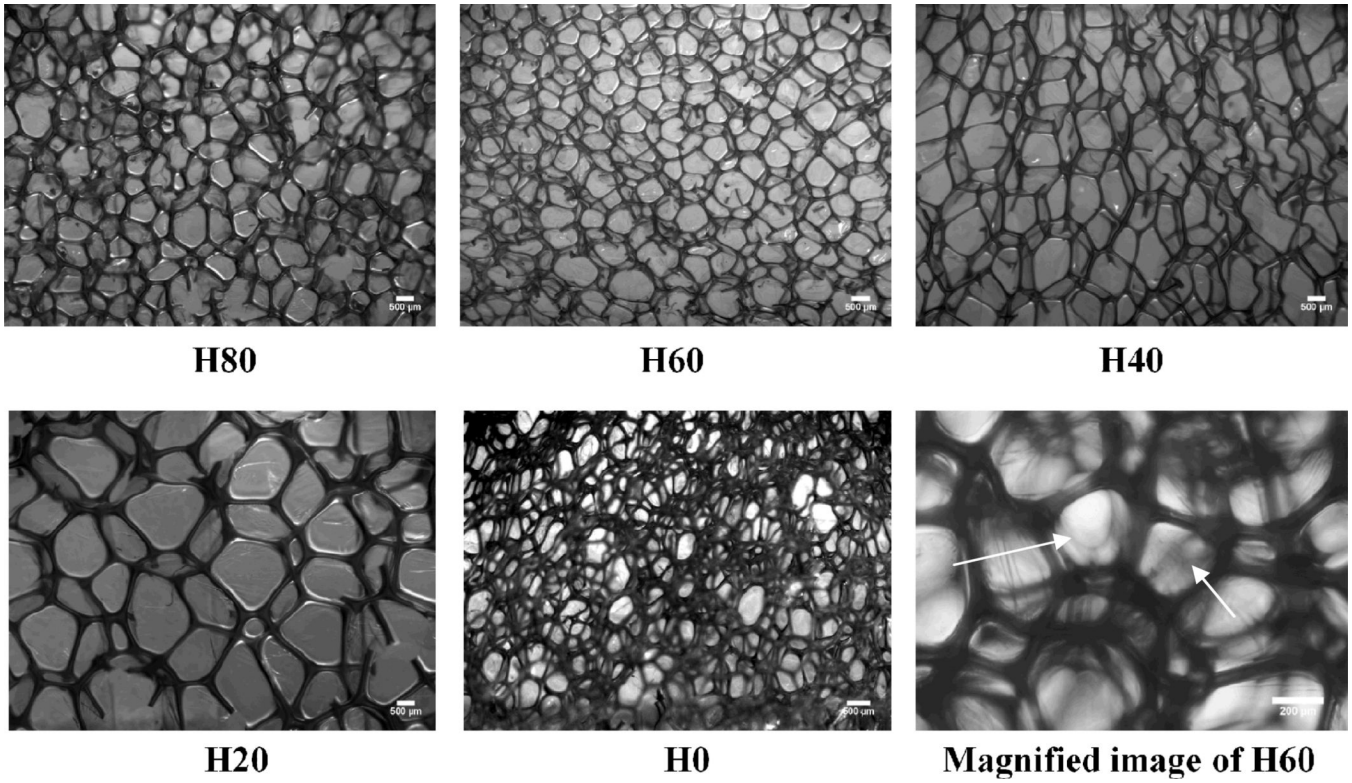

Figure 2.

Representative cell structure of foams for all the formulations H80 through H0. Foams of all formulations show a mixed, closed to open cell structure, with thin cell membranes between struts. The residual thin cell membranes can be seen in the magnified image as marked by arrows. All scale bars are 500 um except the magnified image where the scale bar is 200 um.

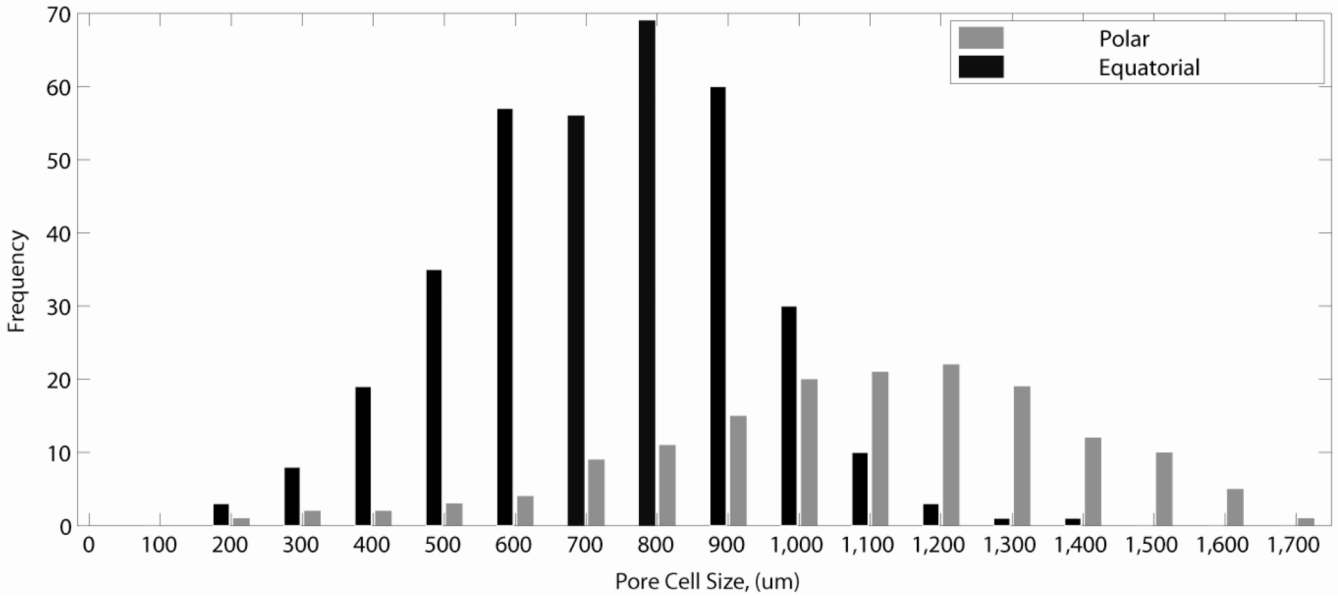

Figure 3.

Histogram showing cell size distribution of H60 foam. It is seen that the pore cells are anisotropic, being taller, approximately 1000 μm, than they are wide, approximately 700 μm. Here equatorial measurements represent lateral diameters of pores, perpendicular to direction of foaming; and the polar measurements represent the longitudinal diameters of pores parallel to the direction of foaming.

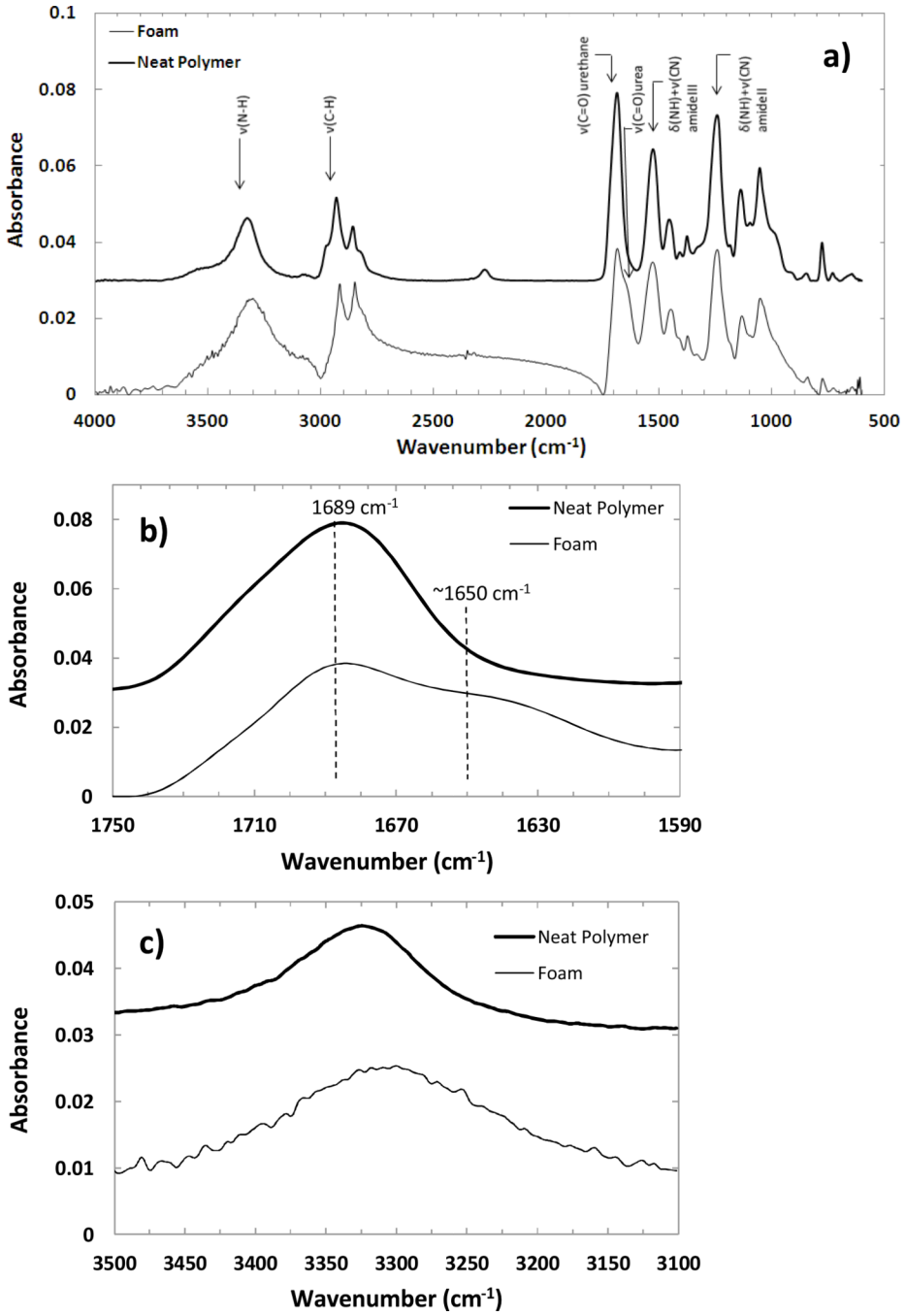

Figure 4.

(a) A comparison between the FTIR-ATR spectra of an unfoamed neat polymer (offset by 0.03 absorbance units) and foam of the corresponding formulation. Some important features are seen: 1) presence of a shoulder in the urethane carbonyl bond (1620–1660 cm^{-1}) indicating presence of urea from chemical foaming with water (b); 2) presence of hydrogen bonding due to urea groups also shows a broadening of the N-H peak (3100–3500 cm^{-1}) (c); and 3) a highly compact and hydrogen bonded structure is estimated as the urethane bond shows a shift to lower wavenumber (1689 cm^{-1}) compared to traditional foams (b).

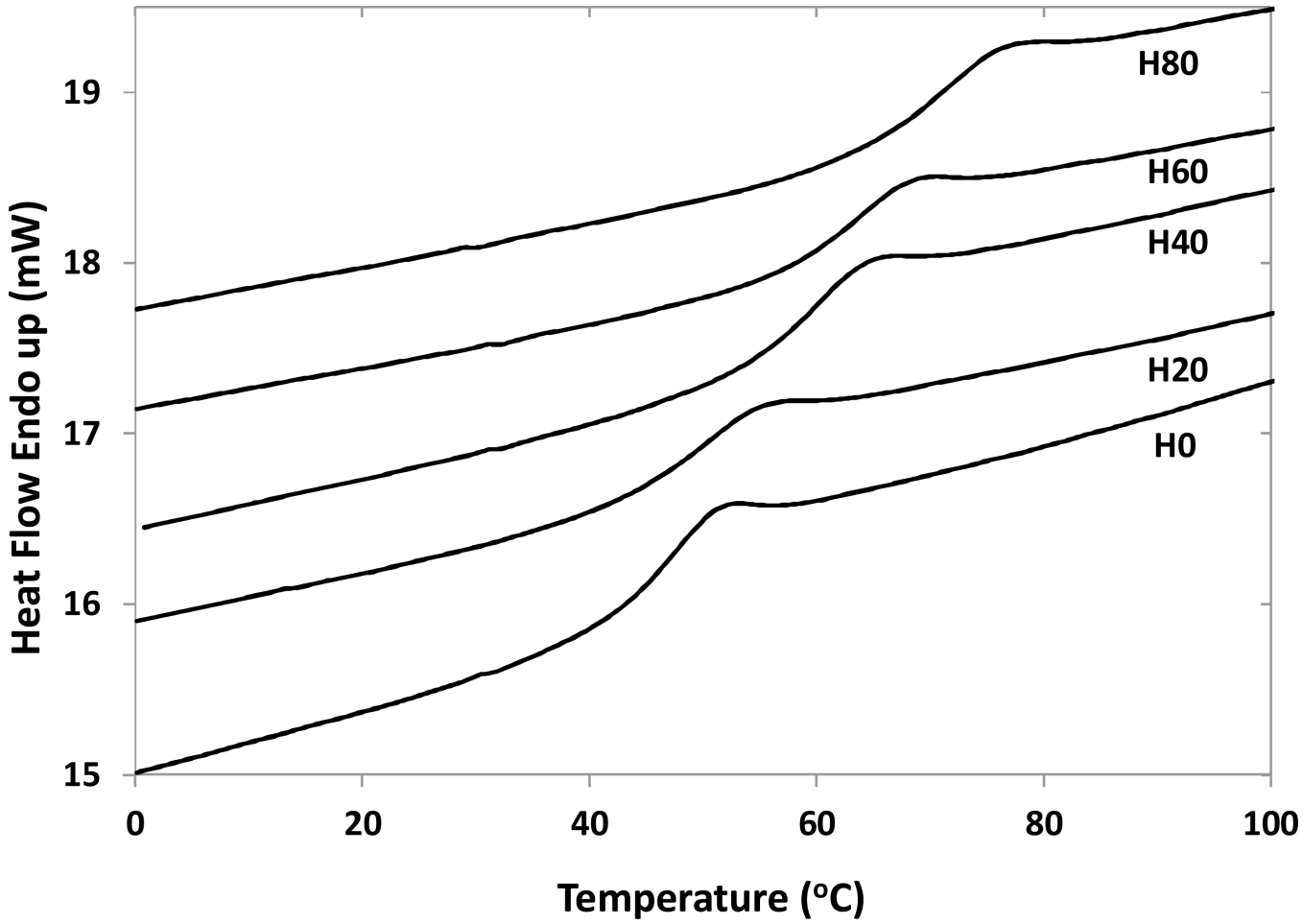

Figure 5.
DSC curves for each foam formulation. A variation in *Tg* of approximately 45–70 °C was achieved by varying the ratio of HPED to TEA in the foam formulation. A higher HPED content gave a higher glass transition value. This is likely due to the increase in rotational steric hinderance due to secondary hydroxyl and increase in crosslink density due to use of tetrafunctional HPED.

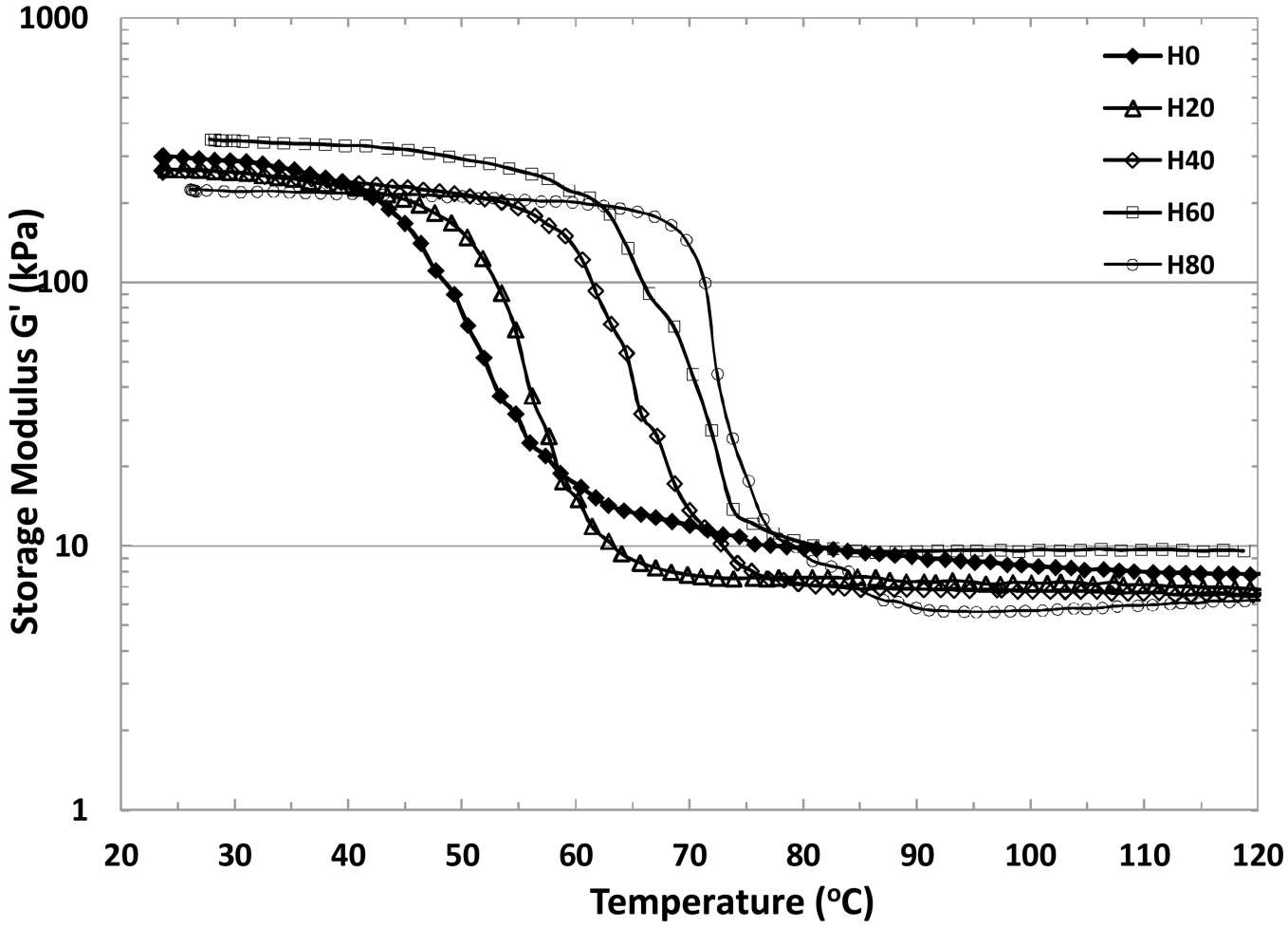

Figure 6.
DMTA curves of H0–H80 samples. Variation in transition temperatures is similar to the DSC results.

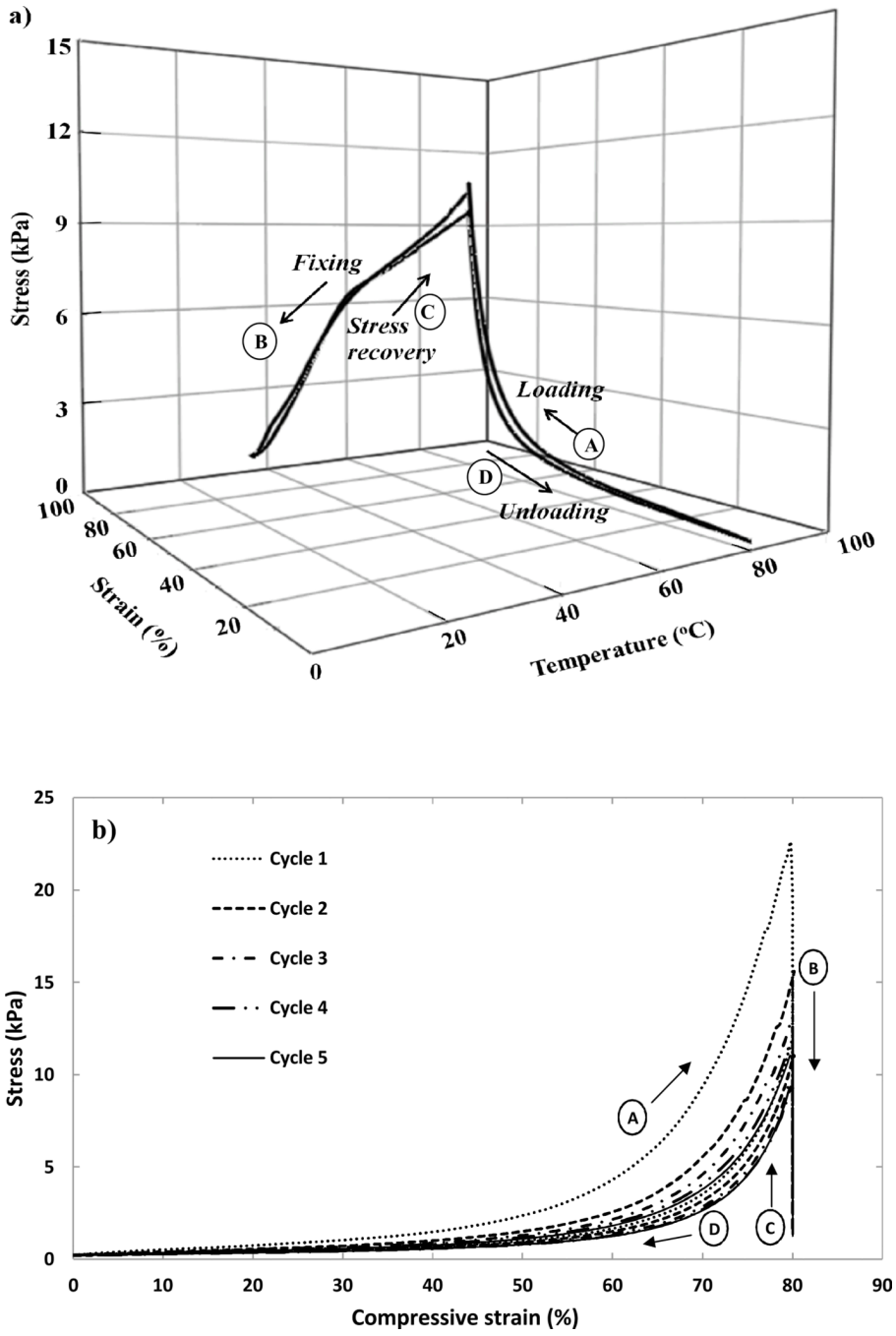

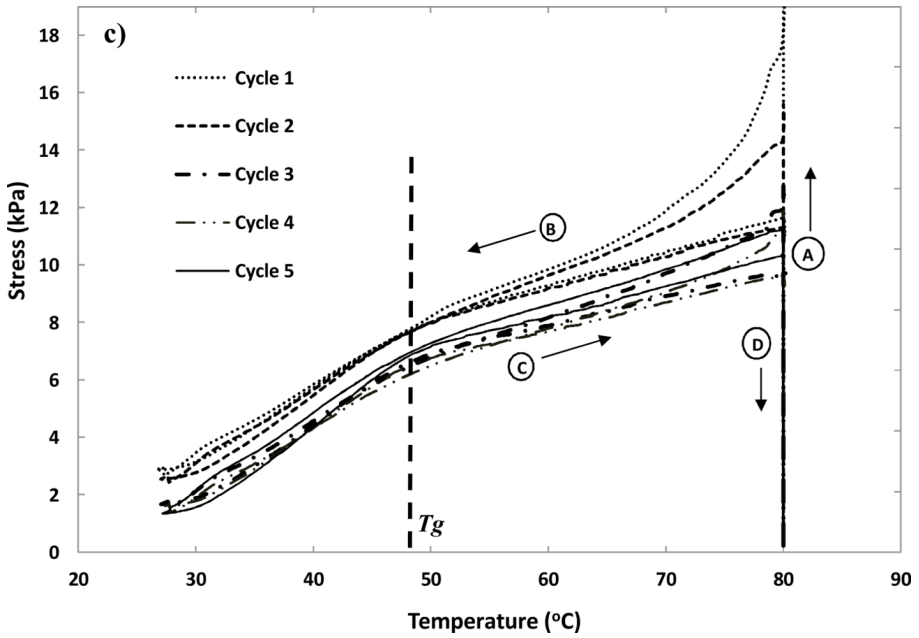

Figure 7.

Shape memory cycles performed on a H20 foam sample (Tg~50 °C) in a constrained stress recovery mode. (a) Four steps of Shape Memory cycle are shown: (A) Loading: The sample heated up to *Tg*+30 °C and a 80% compressive strain applied. (B) Fixing: The compressed sample cooled down to *Tg*−20 °C. (C) Stress Recovery: Sample heated to *Tg*+30 °C. (D) Unloading: Strain released at *Tg*+30 °C. (b) The stress vs. strain behavior of the foams for the 5 cycles. (c) The stress vs. temperature behavior of the foam s for 5 cycles. Stages (A), (B), (C) and (D) on plots represent the steps of loading, fixing, stress recovery and unloading respectively.

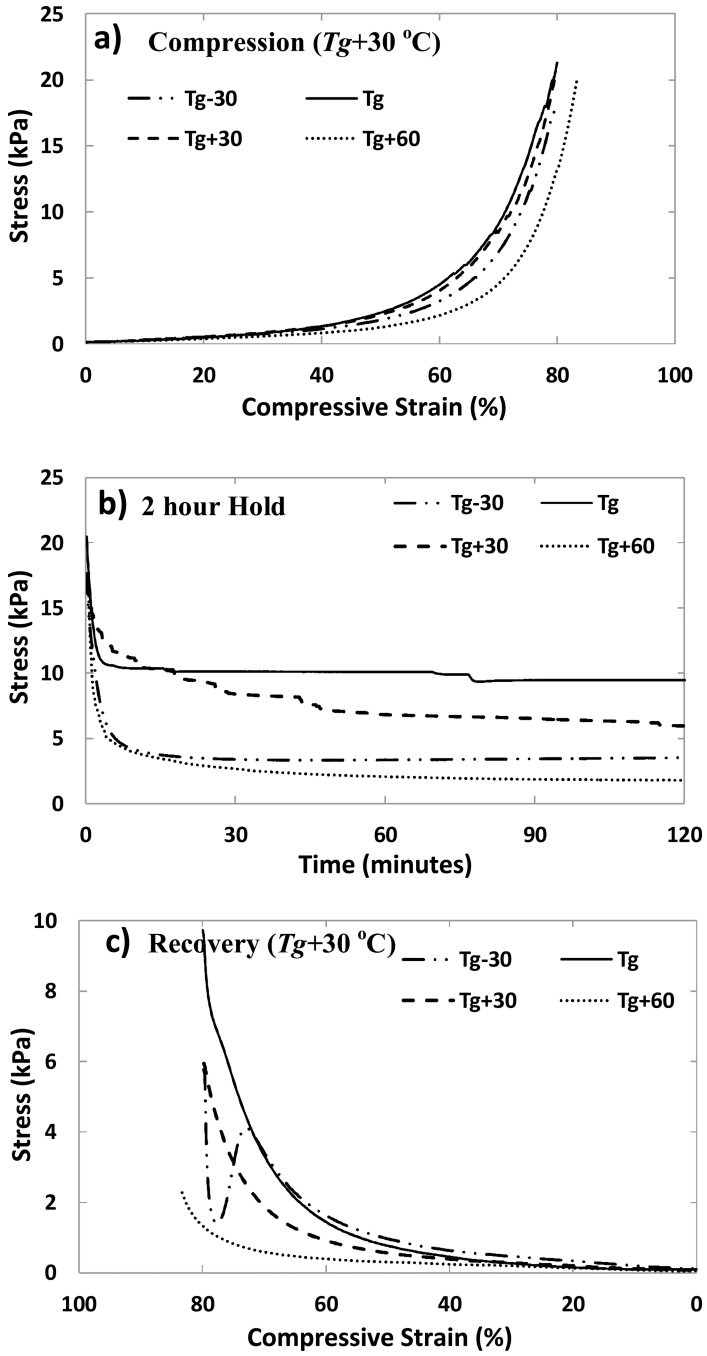

Figure 8.

Shape holding behavior of four H20 foam samples. Four samples named Tg−30, Tg, Tg+30 and Tg+60 are (a) deformed to a 80% compressive strain at *Tg*+30 °C (b) held at specific temperatures of *Tg*−30 °C, *Tg, Tg*+30 °C and *Tg*+60 °C respectively for a period of two hours and (c) unloaded at *Tg*+30 °C.

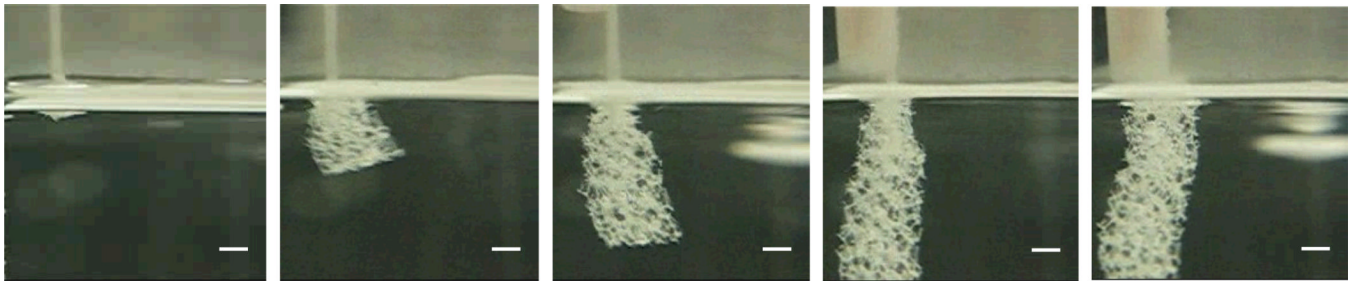

Figure 9.
Demonstration of shape memory behavior of a foam. A 6 mm cylindrical sample of H60 foam was compressed in a mechanical crimper above its Tg and then allowed to cool down to fix the compressed shape. The compressed foam was taped to a rod (seen in the last two panes) and then plunged in a water bath heated to 80 °C. Actuation is seen immediately on contact with water and up to 70 times expansion in volume is observed. Approximate time between panes is 1 sec. Scale bar is 2.5 mm.

Table 1

Scheme of foam formulation. The wt % value represents the net amount of the component in the final foamed polymer.

Sample ID	HDI (wt %)	HPED (wt %)	TEA (wt %)	Water (wt %)	Catalysts (BL-22+T-131 at 2.5:1 wt ratio) (wt %)	Surfactants (DC 4000 +DC5169) (wt %)	Enovate (pph)	OH/NCO ratio
H80	61.8	23.6	4.0	2.7	0.9	7.0	7.4	0.96
H60	63.1	18.1	8.2	2.8	0.9	7.0	7.5	0.96
H40	64.4	12.3	12.6	2.8	0.9	7.0	7.5	0.96
H20	65.8	6.3	17.1	2.9	0.9	7.1	7. 6	0.96
H0	66.7	0.0	22.2	3.0	0.4	7.7	15.4	0.96

Table 2

Summary of key properties of the foams.

Sample ID	Density Top (g cm^{-3})	Density Middle (g cm^{-3})	Density Bottom (g cm^{-3})	Gel fraction (%) [a]	*Tg* (DSC) (°C)	G'_{glassy} at $T_{\delta s}-20$ °C) (kPa) [a]	$G'_{rubbery}$ at $T_{\delta s}+20$ °C (kPa) [a]	T_{onset} (°C)[a]	$T_{\delta s}$ (°C)[a]	ΔT (°C)[a]	*Tan* δ (Peak value) [a]	Volume expansion	% shape recovery after hold for 2 hrs at Tg+60 °C (%) [a]
H80	.017	.018	.026	98 ±1	69	223±18	10±2	64±2	76±1	24±6	0.8±0.1	71	65±7
H60	.021	.021	.022	96±2	61	255±49	11±3	55±1	71±1	31±1	0.9±0.1	68	95±2
H40	.015	.015	.017	96±2	57	212±63	6±2	49±1	64±1	31±7	0.8±0.1	71	94±1
H20	.018	.020	-	97±1	47	235±25	8±1	40±0	57±1	32±3	0.9±0	68	94±1
H0	.023	.019	.021	-	44	259±29	11±1	37±0	52±1	31±1	0.7±0.1	62	99±1

[a] mean ± error (n=3)

Table 3

Results from the biocompatibility study of the foam.

Material	Cytokine Concentration (pg mL^{-1}) [a]				
	IL-1β	IL-6	IL-8	IL-12	TNF-α
media only	2 ± 1	9± 7	846± 896	29± 21	97± 224
PHA	106± 72 (p=0.00075)	414± 125 (p=1.6e-6)	17556± 15030 (p=0.0028)	83± 69 (p=0.015)	310± 295 (p=0.012)
LPS	254± 48 (p=2.2e-8)	529± 21 (p=5.6e-15)	57159± 33715 (p=0.00025)	511± 326 (p=0.00062)	939± 330 (p=4.4e-5)
Foam	17± 45 (p=0.16)	64± 173 (p=0.17)	3689± 8839 (p=0.15)	30± 22 (p=0.014)	100± 213 (p=0.24)

[a] mean ± standard deviation (n=10)